Catalytic Properties of Intermetallic Platinum-Tin Nanoparticles with Non-Stoichiometric Compositions

Yuchen Pei,[†‡] Biying Zhang,[†‡] Raghu V. Maligal-Ganesh,[†‡] Pranjali J. Naik,[†‡] Tian Wei Goh,[†‡] Heather L. McMurdo,[†] Zhiyuan Qi,[†‡] Minda Chen,[†‡] Ranjan K. Behera,[†‡] Igor I. Slowing, [†‡] Wenyu Huang[†‡]*

[†] Department of Chemistry, Iowa State University, Ames, IA, 50011, USA.

[‡] Ames Laboratory, U.S. Department of Energy, Ames, IA, 50011, USA.

* whuang@iastate.edu

ABSTRACT

Intermetallic compounds are unique catalyst platforms for mechanistic studies and industrial applications, because of their ordered structures in comparison to random alloys. Despite the intrinsically defined stoichiometry of intermetallic compounds, compositional deviations can still occur in intermetallic catalysts, and the location of the extra metals differ the catalytic properties of intermetallic compounds with non-stoichiometric composition if the extra metals end up on/near the surface. In this study, we synthesized PtSn intermetallic compounds with accurate stoichiometry and slightly Pt-/Sn-rich compositions. We used furfural hydrogenation and acetylene semi-hydrogenation as probe reactions to investigate the surface structures of PtSn intermetallic catalysts after reduction at different temperatures. Even though the intermetallic PtSn is the major bulk phase among non-stoichiometric compositions, the intermetallic PtSn surface can only be observed under the high-temperature reduction in Sn-rich PtSn intermetallic nanoparticles (iNPs), while the Pt-rich PtSn iNPs shows Pt-rich-surfaces regardless of reduction temperatures.

Four structural models were constructed based on the comprehensive surface and bulk characterizations. This work extends the understanding of intermetallic catalysts with non-stoichiometric compositions to tailor the intermetallic surface structures for catalysis.

KEYWORDS: platinum; tin; furfural hydrogenation; acetylene hydrogenation; surface structure.

1. INTRODUCTION

Surface structure is essential in affecting the catalytic properties of heterogeneous catalysts because the geometric and electronic properties of surface active sites change the adsorption configuration and strength of molecules [1,2]. The rational architecture of heterogeneous catalysts thus relies on the fundamental understanding of the surface structure-catalytic property relationships. However, the near-surface structures of many heterogeneous catalysts are different from their bulk ones, and state-of-the-art techniques cannot easily characterize these thin surfaces under reaction conditions [3]. Therefore, designing well-ordered catalyst platforms and developing *in situ* structural probes are the two strategies to elucidate the dependence of catalytic properties on the surface structures at the molecular level.

Alloy nanoparticles are mostly studied bimetallic catalysts with easily tunable bulk compositions leading to high catalytic activity and selectivity [4-7]. In certain cases, the bulk composition of bimetallic nanoparticles can be synthetically related to their surface structures [8,9]. Additionally, direct modification of the alloy surfaces has been developed to provide more surface structural controls, such as colloidal galvanic replacement [10-12], electrochemical under-potential deposition [13-15], and reaction-driven gas pretreatment [2,9]. However, atoms in alloys can migrate from the surface to bulk phase and *vice versa* [16], leading to the surface segregation and compositional inhomogeneity through alloy nanoparticles [17-19]. The random structures of alloy catalysts complicate the establishment of their structure-property relationships.

Intermetallic compounds, featuring atomic-ordered structures and precise stoichiometry, are ideal platforms for studying the structure-catalysis relationship in comparison to random alloys [20-33]. Intermetallic PdZn [26], PdIn [34], and PdGa [35] catalysts have been reported to show high selectivity in the semi-hydrogenation of acetylene due to the geometric dilution and electronic modification of the precious metal sites at their surfaces. Similar isolation effects of intermetallic compounds have also been practiced on intermetallic PtZn [36] and PtSn [37] in the hydrogenation of nitroarenes. Due to the intrinsic stoichiometry of intermetallic compounds, a slight compositional deviation can dramatically affect their catalytic properties if these extra metals remain on/near the surface. Because the surface structure determines the catalytic properties of heterogeneous catalysts, interesting and important questions for intermetallic catalysts are where the extra metals will be located and how the compositional deviation from the stoichiometric intermetallic compounds can affect their catalytic properties. These questions are crucial for the rational design of intermetallic catalysts.

PtSn nanoparticles are chosen as the model catalyst platform to investigate the effect of non-stoichiometric compositions on the catalytic properties of intermetallic catalysts. Because intermetallic PtSn is a line compound [38], Pt/Sn can maintain a mere 1:1 stoichiometry to form the accurate intermetallic phase. In a recent report, we have revealed that the extra Pt in PtSn iNPs can significantly lower their furfuryl alcohol selectivity in the gas-phase hydrogenation of furfural [24]. The surface-dependent catalytic properties have also been briefly studied over Pt NPs, Pt_3Sn iNPs, and PtSn iNPs in a liquid-phase nitrostyrene hydrogenation reaction [37], and the presence of contiguous Pt sites can lead to the poor selectivity to hydrogenate nitro groups. However, a systematic study has not been conducted to investigate how the extra Pt or Sn in PtSn iNPs can affect their catalytic properties.

Using PtSn iNPs as a model intermetallic catalysts, we endeavor to study the effect of extra Pt or Sn on their structural and catalytic properties. To synthesize the PtSn intermetallic candidates, our group has developed a ship-in-a-bottle method of preparing Pt-based iNPs encapsulated in mesoporous silica shells ($mSiO_2$) [24,39,40]. As-prepared PtSn iNPs can maintain the capping free nature, high thermal stability and ordered structure. This ship-in-a-bottle method also enables the precise composition control of the iNPs by adjusting the amount of the secondary metal precursors. Herein, we demonstrated a structure-catalysis relationship over PtSn iNPs

catalysts with Pt/Sn ratios that slightly deviate from the 1:1 stoichiometry. We also demonstrated that the reduction temperature was a crucial factor to alter the surface structure of the non-stoichiometry PtSn iNPs. Four structural models were suggested by two probe reactions and different characterization techniques to correlate the structure evolution of extra metals in intermetallic PtSn catalysts induced by reduction temperatures.

2. EXPERIMENTAL SECTION

2.1. Synthesis of PtSn iNPs with various ratios.

A proper amount of Pt@mSiO$_2$ seeds (ca. 10 mg, Supporting Information) was taken out from methanol by centrifugation (12000 rpm, 10 min) and re-dispersed in 2.5 mL acetone. The Pt@mSiO$_2$ seeds-acetone solution was transferred to 80 mL tetraethylene glycol (TEG) with the addition of a calculated amount of $SnCl_2 \cdot 2H_2O$ based on the desired Pt/Sn molar ratios in the PtSn iNPs (0.9, 1.0 and 1.2). The resulting TEG solution was protected in argon, heated to 260 °C in 45 min with stirring, and then to 280 °C in 20 min. The solution was maintained at 280 °C for 2 h. After reaction and cooling to room temperature, 80 mL acetone was added to the TEG solution, and PtSn iNPs were centrifuged down at 12000 rpm for 10 min. After washing 3 times with ethanol, PtSn iNPs were dried in vacuum at room temperature and calcined at 500 °C in air for 4 h to remove organic capping agents. The PtSn iNPs were then reduced at 300 or 500 °C for 2 h in 10% H_2/Ar (a total flow of 50 mL min^{-1}), denoted as PtSn-300 or PtSn-500 iNPs. The actual Pt/Sn ratios of as-prepared PtSn iNPs were confirmed by inductively coupled plasma-mass spectroscopy (ICP-MS).

2.2. Catalytic probe reactions for PtSn iNPs.

The catalytic property of PtSn iNPs was studied using a plug flow reactor. For furfural hydrogenation, 0.3-0.5 mg PtSn iNPs were diluted with 200 mg quartz sands and placed into a U-shaped quartz tube attached to the reactor. A gas feed of furfural(He)/H_2 was maintained as 0.023/11.4 mL min^{-1}, where 8.6 mL min^{-1} He flow were used to carry furfural from a bubbler into the reactor. PtSn iNPs catalysts were calcined at 500 °C in air for 4 h, and reduced *in situ* at either 300 or 500 °C for 2 h in 10% H_2/He (a total flow of 50 mL min^{-1}) before every furfural

hydrogenation. The gas contents were monitored and quantified using gas chromatography (GC) equipped with a capillary column (EC-5, 30 m × 0.32mm × 0.25 μm) and a flame ionization detector (FID). For acetylene semi-hydrogenation, 2 mg PtSn iNPs was used, and gas feed of $C_2H_2/C_2H_4/H_2$/He was controlled as 0.15/15/1.5/13.5 mL min^{-1}. The gas contents were monitored and quantified using a GC equipped with a capillary column (HP PLOT/Q, 30 m × 0.32 mm × 0.2 mm) and a FID. For the mass diffusion limit test, we used monometallic Pt@mSiO_2 to test the flow reactors over furfural hydrogenation at the above reaction conditions. The catalyst amount of Pt@mSiO_2 was varied from 0.3 to 1.2 mg.

2.3. Characterization.

Powder X-ray diffractions (PXRD) patterns of the samples were acquired by a STOE Stadi P powder diffractometer or a Bruker D8 Advance Twin diffractometer, Cu K_α radiation (40 kV, 40 mA, λ = 0.1541 nm). Transmission electron microscopy (TEM), high-angle annular dark field scanning TEM (HAADF-STEM), and elemental mapping analysis were investigated using a Tecnai G2 F20 electron microscope equipped with energy-dispersive X-ray spectroscopy (EDS) detector (Oxford INCA EDS) and a Titan Themis 300 probe corrected TEM with a Super-X EDS detector. The actual metal loadings in the PtSn iNPs were measured by ICP–MS (X Series II, Thermo Scientific). All metals in samples were digested completely using aqua regia after removing the mesoporous silica. Diffuse reflectance infrared Fourier transform spectroscopy (DRIFTS) was conducted using an Agilent Cary 670 Fourier transform infrared spectrometer equipped with a linearized HgCdTe (MCT) detector, a Harrick diffuse reflectance accessory, and a Praying Mantis high-temperature reaction chamber. CO was the probe molecule. 10-20 wt.% sample was diluted with KBr before the measurement. 5% CO/He mixture (50 mL min^{-1} in total flow) was used to saturate PtSn iNPs surface and 50 mL min^{-1} He was used to remove gas CO remnants. The spectra were obtained at the steady state of CO adsorption peak after removing all gas CO. X-ray absorption fine structure spectroscopy (XAFS) and X-ray absorption near edge spectroscopy (XANES) spectra were measured in transmission mode (Pt L_3 edge = 11564 eV and Sn K edge = 23220 eV) at 9-BM-B and 20-BM-B beamlines of the Advanced Photon Source in Argonne National Laboratory. XAFS of reference samples were collected using pure finely ground powders homogeneously dispersed on polyimide Kapton tape. While the PtSn iNPs (diluted with boron nitride) were pressed into a pellet fit to a hole embedded in a sample holder,

reference platinum was acquired simultaneously with each measurement for energy calibration. The Athena program, which is an interface to IFEFFIT and FEFFIT, was used for smoothing raw data and converting spectra from energy to *k* space. All the extended X-ray absorption fine structures (EXAFS) data fittings were performed with a k^3 weight in *R* space by Artemis program from the same package using the quick shell theory of related Pt and Sn coordination. The Pt dispersions of catalysts were measured over Micromeritics AutoChem II 2920 equipped with a thermal conductivity detector. All Pt-/Sn-rich PtSn catalysts are freshly reduced at the targeted temperatures, and *in situ* reduced again (150 °C) before the measurement at 30 °C. For Pt and $Pt_{1.0}Sn@mSiO_2$, the Pt dispersion was measured over Micromeritics 3Flex.

3. RESULTS AND DISCUSSION

The PtSn iNPs were the model catalysts synthesized via the ship-in-a-bottle strategy as reported in our previous work [24,37,39]. PtSn model iNPs have a core-shell structure where PtSn intermetallic cores (ca. 18 nm) are encapsulated inside the $mSiO_2$ shells (ca. 10 nm in thickness) as shown by the scheme in Figure 1a. Figure 1b and c are TEM images of the PtSn iNPs encapsulated in $mSiO_2$. Noting that the formation of accurate PtSn intermetallic phase was completed and confined within the $mSiO_2$ shells, this synthesis architecture ensures the atomic level homogeneity of the PtSn composition in individual NPs [24,37]. The homogeneity of the intermetallic phase at single particle level renders the PtSn iNPs in this study as model catalysts with structural clarification in comparison to intermetallic compounds prepared by general impregnation method. The surface composition of these $mSiO_2$-encapsulated PtSn iNPs is also stable in the reducing environment up to 500 °C as evidenced by in situ ambient-pressure X-ray photoelectron spectroscopy in our previous work [37]. The average pore size of $mSiO_2$ shells is 2.2-2.5 nm where small molecules can access the PtSn intermetallic cores to initiate chemical reactions, such as furfural and nitroarenes [24,37]. The detailed catalysts characterization was included in the Supporting Information as well as in our previous reports [24,37,39].

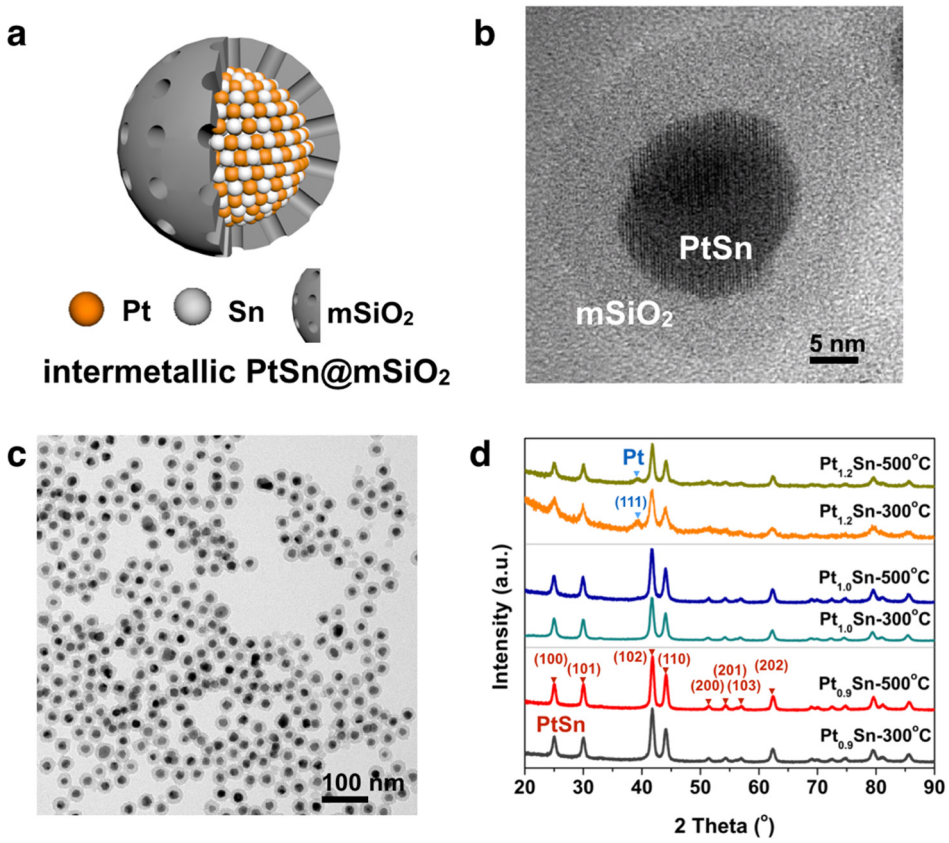

Figure 1. (a) Structural illustration of our model core-shell PtSn iNPs catalysts. (b, c) TEM images of $Pt_{1.0}Sn$ iNPs after 500 °C calcination and 300 °C reduction with different magnification. No aggregation of iNPs was observed after the thermal treatment. (d) PXRD patterns of $Pt_{0.9}Sn$, $Pt_{1.0}Sn$, and $Pt_{1.2}Sn$ iNPs reduced at 300 and 500 °C. Blue/red triangles indicate the characteristic diffraction peaks in Pt/intermetallic PtSn standard patterns.

The ship-in-a-bottle strategy can provide precise control of the composition of the individual bimetallic particle by altering the ratios of two metal precursors [39]. Bulk Pt/Sn ratios of PtSn iNPs can thus be finely tuned with extra Pt or Sn departing from the intrinsic 1:1 stoichiometry. We varied the extra metal ratios from 10-20 mol.% capable of covering the whole surfaces of a 20 nm PtSn spherical particle (theoretical dispersion: 7 mol.%) [41]. Due to the high incorporation efficiency of secondary metals using the ship-in-a-bottle method, the molar ratios of Pt seed to the secondary metal precursors determine the compositions of the final bimetallic

NPs. We thus prepared $Pt_{1.2}Sn$, $Pt_{1.0}Sn$ and $Pt_{0.9}Sn$ iNPs with precise Pt/Sn ratios, and their bulk compositions were confirmed by ICP-MS as 1.16 ± 0.03, 0.99 ± 0.04 and 0.91 ± 0.03, close to the respective precursor ratios (Table S1 in Supporting Information). In the ship-in-a-bottle method, Pt seeds are essential to facilitate the reduction of secondary metal precursors in the tetraethylene glycol solvent [39]. For random alloy NPs, PtPd NPs synthesized by this method could have flexible Pd/Pt ratios from 0.5 to 2.0 [39]. However, we observed a restricted bimetallic ratio in intermetallic PtSn NPs likely due to the high thermodynamic stability and restricted stoichiometry of PtSn intermetallic phase (i.e. the exothermic formation of PtSn phase) [42]. We found that we could not deposit more than 10% extra Sn on Pt seeds for Sn-rich PtSn iNPs, so $Pt_{0.9}Sn$ is the highest Sn content we could reach. For Pt-rich PtSn iNPs, the major crystal phase can only fall into intermetallic Pt_3Sn when Pt/Sn ratio approaches 3/1. Even though the composition of PtSn iNPs cannot be freely tuned, this restricted composition of PtSn iNPs exemplifies the ordered thermodynamically stable structures of intermetallic compounds in comparison to random alloys.

Due to the protection of the mesoporous silica shells, these PtSn iNPs have high thermal stability against aggregation (Figure 1a, b, and c). We first calcined these PtSn iNPs at 500 °C in air to remove surface capping agents. During the calcination, PtSn iNPs transform to phase-segregated Pt and SnO_2 particles (Pt-SnO_2 particles) [24]. Our previous studies have demonstrated the recovery of ordered intermetallic PtSn phase for Pt-SnO_2 particles (Pt:Sn = 1:1) reduced at 300 °C [37]. With Pt:Sn ratio deviates from 1:1, the recovery of the intermetallic PtSn phase could lead to different surface structures depending on the Pt/Sn ratio after we reduced these Pt-SnO_2 particles at different temperatures. We thus applied two reduction temperatures for the reconstruction of PtSn iNPs at 300 and 500 °C. These PtSn iNPs reduced at the two temperatures were denoted as Pt_xSn-300 and Pt_xSn-500 (x=0.9, 1.0 and 1.2). PXRD patterns of $Pt_{1.0}Sn$ iNPs reduced under different temperatures show that the intermetallic PtSn phase was formed after either 300 or 500 °C reductions (Figure 1d). The PXRD of Pt-rich $Pt_{1.2}Sn$-300 iNPs majorly displays the PtSn intermetallic phase despite a small amount of monometallic Pt phase indicated by the blue triangle in Figure 1d. The Pt phase in $Pt_{1.2}Sn$-500 was suppressed after reducing at 500 °C. For stoichiometric $Pt_{1.0}Sn$ and Sn-rich $Pt_{0.9}Sn$ iNPs, we only observed the intermetallic PtSn phase from the PXRD patterns regardless of reduction at 300 or 500 °C. Unlike alloys, Pt

phase can be clearly distinguished from the intermetallic PtSn phase in $Pt_{1.2}Sn$ with only 10-20% extra Pt than the 1:1 stoichiometry.

To visualize the location of extra Pt and Sn in PtSn iNPs, we acquired elemental mappings and EDS line scans for PtSn iNPs (Figure 2) by HAADF-STEM. A Pt/Pt-rich core with a PtSn shell structure was observed in $Pt_{1.2}Sn$-300 iNPs (Figure 2b). After the reduction at 500 °C, $Pt_{1.2}Sn$-500 iNPs have a more homogeneous mixing of Pt and Sn than $Pt_{1.2}Sn$-300 iNPs, while a spike of Pt signal was still observed, indicating the presence of Pt domains in the NP (Figure 2d). This observation is consistent with the suppressed but obvious Pt PXRD peak from $Pt_{1.2}Sn$-500 iNPs (Figure 1d). $Pt_{0.9}Sn$-300 iNPs also have a Pt/Pt-rich core with a PtSn shell structure (Figure 2f) that is less obvious in comparison to $Pt_{1.2}Sn$-500 iNPs. Upon the reduction at 500 °C, $Pt_{0.9}Sn$-500 iNPs show a relatively homogeneous distribution of Pt and Sn signals through the entire NP (Figure 2h). The inserted HAADF-STEM images in Figure 2 also show the heterogeneity of Pt and Sn distributions in Pt-rich $Pt_{1.2}Sn$ iNPs (a bright core) in comparison to Sn-rich $Pt_{0.9}Sn$ iNPs.

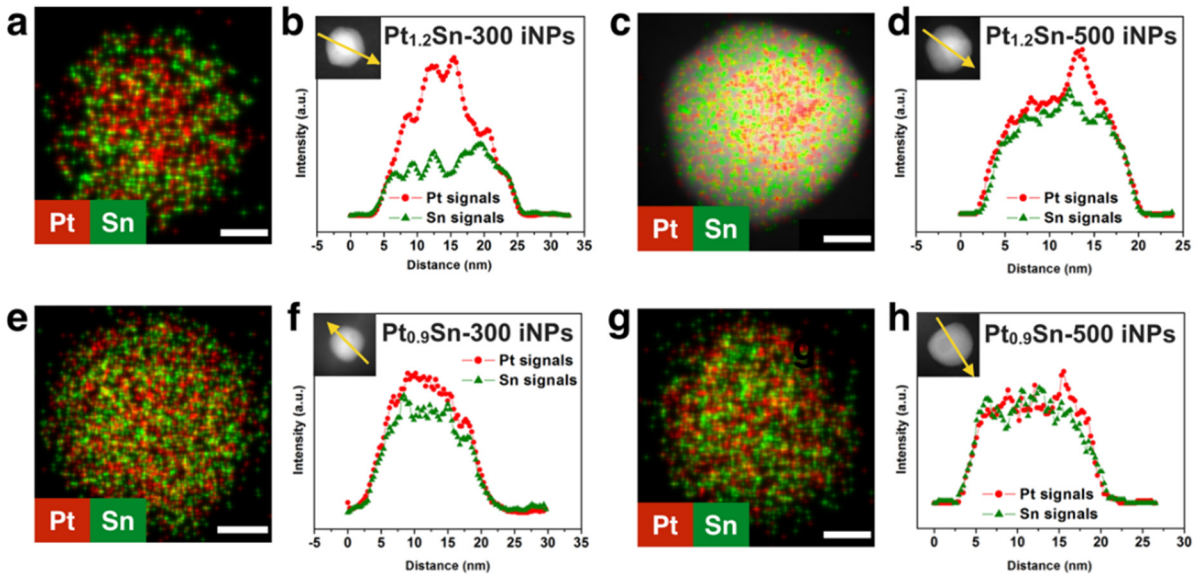

Figure 2. Elemental mappings and EDS line scan of representative $Pt_{0.9}Sn$ and $Pt_{1.2}Sn$ iNPs reduced at 300 and 500 °C. The scale bars in Figure a, c, e, and g are 5 nm. The EDS line scans of (b) $Pt_{0.9}Sn$-300, (d) $Pt_{0.9}Sn$-500, (f) $Pt_{1.2}Sn$-300, and (h) $Pt_{1.2}Sn$-500. The red dots and green triangles are Pt and Sn signals of PtSn iNPs. The inserts in Figure b, d, f, and h are HAADF-STEM images of (a) $Pt_{1.2}Sn$-300, (c) $Pt_{1.2}Sn$-500, (e) $Pt_{0.9}Sn$-300, and (g) $Pt_{0.9}Sn$-500.

We also acquired EXAFS spectra at Pt L_3 and Sn K edges for Pt_xSn iNPs as shown in Figure S1-2 and Table S2-3 to obtain the ensemble information and validate the HAADF-STEM results. The white lines in all PtSn iNPs at Pt L_3 edge shows a shift to high-energy in comparison to that of Pt foil, due to the formation of PtSn intermetallic phase (Figure S1a). The white lines of all PtSn iNPs at Sn K edge position at similar energy in comparison to that of a Sn foil (Figure S1b) [43,44]. $Pt_{1.0}Sn$ and Sn-rich $Pt_{0.9}Sn$ iNPs have the Pt-Pt and Pt-Sn coordination numbers close to 2 and 4 at Pt L_3 edge (Table S2-3), as well as the Sn-Pt coordination number close to 6 at Sn K edge [45]. Although we noticed that the fitted Pt-Sn coordination number (4) deviates from the theoretical value (6), which might need to be calibrated by using a pure phase bulk PtSn intermetallic compounds. However, the trend in coordination number could still be used to understand the structure change of the intermetallic NPs. The Pt-Pt, Pt-Sn, and Sn-Pt coordination numbers of $Pt_{1.0}Sn$ and Sn-rich $Pt_{0.9}Sn$ iNPs are very close, indicating the formation of ordered PtSn phase in $Pt_{1.0}Sn$ and $Pt_{0.9}Sn$ iNPs regardless of the different reduction temperatures. On the other hand, we observed a significant deviation in the coordination numbers for the Pt-rich $Pt_{1.2}Sn$-300, in which the Pt-Pt, Pt-Sn, and Sn-Pt coordinations were fitted as 4.6(0.3), 3.3(0.1) and 4.5(0.2), respectively. The large deviation of Pt-Pt and Sn-Pt coordination numbers from their theoretical values of 2 and 6 indicates the significant Pt aggregates in the bulk phase of $Pt_{1.2}Sn$-300 iNPs. This observation agrees with the presence of concentrated Pt cores as observed in the HAADF-STEM images and EDS line scan profiles (Figure 2a and b). After reduction at 500 °C, the Pt-Pt and Sn-Pt coordinations of $Pt_{1.2}Sn$-500 iNPs were fitted as respective 2.7(0.3) and 5.5(0.2), approaching their corresponding theoretical values of 2 and 6, indicating the bulk structure of the Pt-rich particles transforms to the major PtSn intermetallic phase at 500 °C.

The PXRD, EDS, and EXAFS results demonstrate the structure evolution of PtSn intermetallic compounds with non-stoichiometry compositions upon reductions. However, these characterization techniques cannot provide detailed information on their surface structures. Despite that Pt/Pt-rich core was observed in $Pt_{1.2}Sn$-300, the other catalysts did not show a major structural difference to trace the location of the extra Pt and Sn. We further used furfural hydrogenation as a probe reaction to investigate the surface structures of these PtSn iNPs

reduced at different temperatures. To our surprise, these four catalysts beheld different catalytic properties as shown in Figure 3 and Figure S3. In a previous report, we had demonstrated that $Pt_{1.0}Sn$-300 iNPs are highly active and selective (>99%) in the hydrogenation of furfural to furfuryl alcohol due to the straight-up adsorption geometry of furfural molecules on the intermetallic PtSn(110) facet [24]. Herein, $Pt_{1.2}Sn$ and $Pt_{0.9}Sn$ iNPs show different catalytic properties in furfural hydrogenation depending on their compositions and reduction temperatures. Using catalysts that contain similar amounts of Pt and comparing their performance at the 220 °C reaction temperature, Pt-rich $Pt_{1.2}Sn$ iNPs have high activity (20% conversion) and 95% selectivity to furfuryl alcohol after reduction at either 300 or 500 °C, while Sn-rich $Pt_{0.9}Sn$ iNPs have variable catalytic properties depending on the reduction temperatures. $Pt_{0.9}Sn$-300 has high activity (20% conversion) and 95% selectivity similarly to that of $Pt_{1.2}Sn$ iNPs. However, the 500 °C reduction significantly depresses the activity of $Pt_{0.9}Sn$-500 iNPs (ca. 5% conversion) with enhanced selectivity (>99%) as shown in Figure S3a. To obtain the catalytic benchmark, we also tested monometallic Pt@mSiO_2 NPs and stoichiometric $Pt_{1.0}Sn$ iNPs for the furfural hydrogenation. $Pt_{1.0}Sn$ iNPs showed a high selectivity of >99%; whereas only 30% selectivity was observed on the monometallic Pt@mSiO_2 catalyst. We summarized the apparent activation energy of Pt-Sn iNPs for furfural hydrogenation in Figure 3a and Figure S4-5 to compare the different catalytic properties. To exclude the mass transfer limitation and obtain accurate activation energy values, we varied the amount of Pt@mSiO_2 and observed a linear relationship between the conversion and the amount of used catalyst as shown in Figure S6-7. Two sets of catalysts can be classified based on their apparent activation energy values: i) Pt-rich $Pt_{1.2}Sn$-300, $Pt_{1.2}Sn$-500, and Sn-rich $Pt_{0.9}Sn$ iNPs-300 iNPs have activation energies close to that of Pt control (16-18 kJ mol^{-1}), and they show higher selectivity to furfuryl alcohol (90% at 220 °C) than monometallic Pt@mSiO_2 NPs but not as high as $Pt_{1.0}Sn$ iNPs. $Pt_{1.2}Sn$-500 iNPs show the lowest activation energy among all PtSn iNPs samples. ii) Differently, Sn-rich $Pt_{0.9}Sn$-500 iNPs have similar activation energy and high selectivity in comparison to $Pt_{1.0}Sn$-300 iNPs with well-ordered intermetallic structures (23-28 kJ mol^{-1}). The TOFs of these Pt-Sn iNPs in furfural hydrogenation were also calculated as shown in Figure S8. The Pt-Sn iNPs have 2 to 7-fold higher TOFs than pure Pt exemplifying the promotion effect of bimetallic Pt-Sn in furfural hydrogenation. The Pt-rich $Pt_{1.2}Sn$ catalysts have similar TOFs (0.20 s^{-1}) regardless of the reduction temperatures. The Sn-rich $Pt_{0.9}Sn$ iNPs show dramatically lower TOFs after the

reduction at 500 °C (0.37 s^{-1} for $Pt_{0.9}Sn$-300 iNPs, and 0.11 s^{-1} for $Pt_{0.9}Sn$-500 iNPs). The highest TOF value was obtained over Sn-rich $Pt_{0.9}Sn$-300 iNPs among all catalysts. We thus speculate that the reduction temperature can induce the reconstruction of the extra metals in Pt-Sn iNPs endowing different surface structures. The surface of $Pt_{0.9}Sn$-500 iNPs can reflect the ideal PtSn intermetallic structure and is largely different from that of $Pt_{1.2}Sn$-300, $Pt_{1.2}Sn$-500, and $Pt_{0.9}Sn$-300 iNPs with more Pt-rich surfaces. It is worthwhile to note that we cannot exclude the possibility of PtSn surface reconstruction under reaction conditions due to the interactions between reactant molecules and PtSn surface atoms.

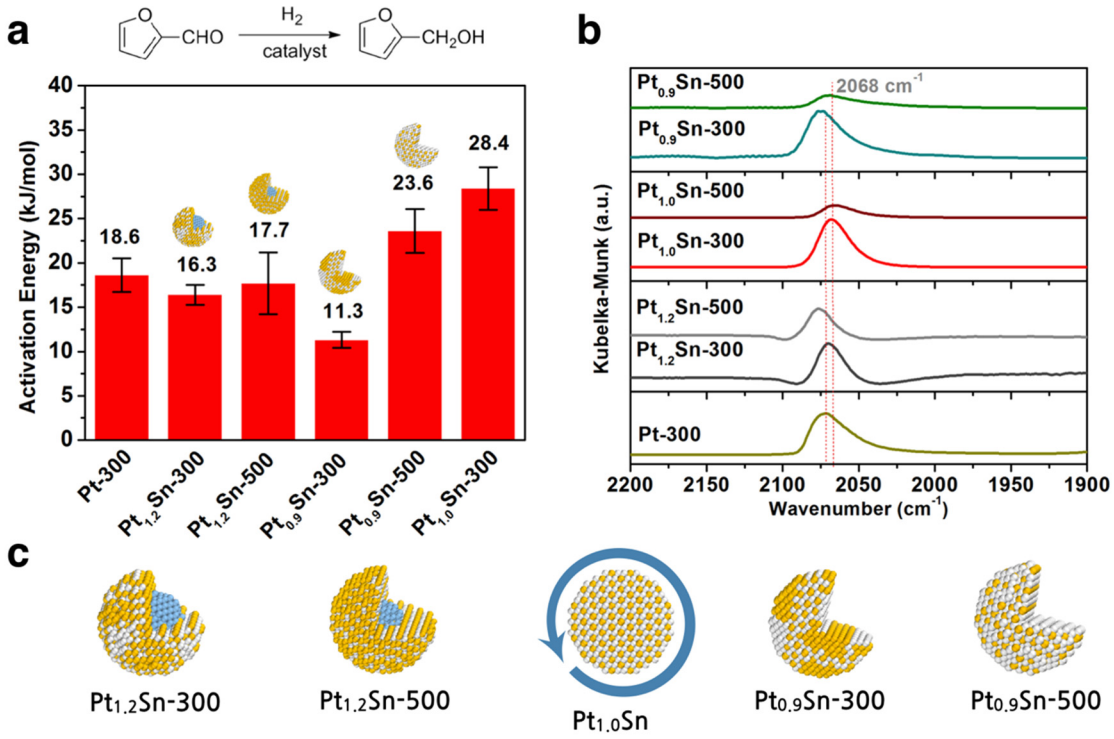

Figure 3. (a) Apparent activation energy of furfural hydrogenation over Pt@mSiO_2, $Pt_{0.9}Sn$, $Pt_{1.0}Sn$, and $Pt_{1.2}Sn$ iNPs reduced at 300 and 500 °C. 0.3-0.5 mg catalyst was used in furfural hydrogenation with a gas feed of furfural/H_2=0.023/11.4 mL min^{-1}. A He flow of 8.6 mL min^{-1} carries furfural vapor from a bubbler into the reactor. (b) CO-DRIFTS spectra for Pt@mSiO_2, $Pt_{0.9}Sn$, $Pt_{1.0}Sn$, and $Pt_{1.2}Sn$ iNPs reduced at 300 and 500 °C. (c) Proposed structural models for $Pt_{1.2}Sn$-300, $Pt_{1.2}Sn$-500, $Pt_{1.0}Sn$, $Pt_{0.9}Sn$-300, and $Pt_{0.9}Sn$-500 iNPs. The yellow/white dots represent Pt/Sn atoms, and the blue dots exclusively represent the Pt atoms in the core area.

DRIFTS study was used to investigate the surface structures of PtSn iNPs with CO as the probe molecule (Figure 3b). In all DRIFTS spectra of PtSn iNPs, only one mode of atop CO band was observed after the catalyst surface was saturated with CO molecules. The respective peak shifts of atop CO mode can be readily divided into two categories matching well to the two activation energy sets in the furfural hydrogenation. Due to the electron donation from Sn to Pt, CO molecules adsorbed on $Pt_{1.0}Sn$-300 iNPs display a shift to a low wavenumber (2068 cm^{-1}) in comparison to those on Pt (2073 cm^{-1}) in accord with our previous studies [37]. We also reduced $Pt_{1.0}Sn$ iNPs to 500 °C, and the peak position of atop CO on $Pt_{1.0}Sn$-500 iNPs remains the same despite a decrease in intensity, which indicates that $Pt_{1.0}Sn$ iNPs can have a relatively stable surface structure derived from the well-ordered intermetallic phase. The peak positions of atop CO adsorbed on Pt and $Pt_{1.0}Sn$ can serve as two benchmarks to evaluate the surface structures of Pt- and Sn-rich Pt-Sn iNPs. The CO adsorption features of Sn-rich $Pt_{0.9}Sn$-500 iNPs resemble that of $Pt_{1.0}Sn$ iNPs, indicating the presence of an ideal PtSn intermetallic surface due to ordering effect after the 500 °C reduction. Different from $Pt_{1.0}Sn$ iNPs, CO molecules adsorbed on Pt-rich $Pt_{1.2}Sn$-300, $Pt_{1.2}Sn$-500, and Sn-rich $Pt_{0.9}Sn$-300 iNPs show shifts to high wavenumbers, demonstrating the presence of contiguous surface Pt sites. The contiguous surface Pt sites could also explain their high activity but lower selectivity in furfural hydrogenation.

Combining EDS mapping and line scan, EXAFS, DRIFTS, and furfural hydrogenation results, we proposed the structural models of the Pt-Sn iNPs with non-stoichiometric compositions as shown in Figure 3c. The stoichiometric $Pt_{1.0}Sn$ iNPs show homogeneous distributed Pt and Sn atoms because of the intrinsic intermetallic structures of PtSn. $Pt_{1.2}Sn$-300 iNPs have contiguous Pt sites on the surface with a large Pt core, which can explain their similar catalytic properties as monometallic Pt@$mSiO_2$ NPs. After reduction at 500 °C, smaller Pt cores and more homogeneous distribution of Pt can be induced in $Pt_{1.2}Sn$-500 iNPs likely leading to the formation of Pt-rich top-layer structures over a PtSn intermetallic sublayer. Similar Pt/PtSn core/shell structures [33] have been reported with enhanced electrocatalytic activities, as well as other highly active intermetallic PtZn with a Pt-rich shell [30] and Pt skinned Pt/Pd NPs [46,47]. The surface Pt enrichment at the high temperature (i.e. 500 °C) can be attributed to the higher surface energy of PtSn than monometallic Pt [48]. For Sn-rich samples, $Pt_{0.9}Sn$-300 iNPs display similar contiguous Pt sites on the surface. However, the 500 °C reduction can homogenize the structures of $Pt_{0.9}Sn$-500 iNPs and lead to a well-ordered PtSn surface partially covered by Sn,

agreeing to their similar activation energies but lower activity in comparison to stoichiometric $Pt_{1.0}Sn$ iNPs (Figure 3a) in the furfural hydrogenation. Moreover, the high mobility and low surface energy of Sn could explain that extra Sn would prefer to stay on the PtSn surface of $Pt_{0.9}Sn$-500 iNPs [49]. We also acquired the Pt dispersion values to validate these four models following the order of Pt >> ($Pt_{0.9}Sn$-300 ~ $Pt_{1.2}Sn$-500 ~ $Pt_{1.0}Sn$-300 ~ $Pt_{1.2}Sn$-300) > $Pt_{0.9}Sn$-500 (Table S4). Pt dispersion of $Pt_{1.2}Sn$ iNPs did not vary regardless of the reduction temperature. However, the Pt dispersion was significantly decreased over the Sn-rich $Pt_{0.9}Sn$ iNPs after 500 °C reduction correlated to the higher surface Sn coverage.

To further validate these structural models, especially to investigate the surface homogeneity, we used acetylene semi-hydrogenation as another probe reaction. Acetylene semi-hydrogenation is sensitive to the presence of ensemble (contiguous) Pt sites that have been widely studied over single-sited and intermetallic catalysts [26,50,51]. The desired product in the acetylene semi-hydrogenation is ethylene. However, contiguous Pt sites favor the further hydrogenation of ethylene to ethane and decrease the selectivity in the acetylene hydrogenation [52]. Our structure model in Figure 3c conjectures that the presence of Pt contiguous sites on $Pt_{1.2}Sn$-300, $Pt_{1.2}Sn$-500, and $Pt_{0.9}Sn$-300 iNP would lead to higher conversion and lower selectivity to ethylene, in agreement to our catalytic observation as shown in Figure 4. On the contrary, the Sn-rich $Pt_{0.9}Sn$-500 shows a dramatically enhanced selectivity due to the homogeneous dilution of Pt in the intermetallic PtSn structures. The low activity in $Pt_{0.9}Sn$-500 also confirms that the intermetallic surface is partially covered with Sn (Figure 4a). $Pt_{1.0}Sn$-300 catalyst also shows high selectivity to ethylene due to its ordered PtSn intermetallic surface (Figure S9). The acetylene semi-hydrogenation results readily correspond to the proposed structural models. Using acetylene semi-hydrogenation and furfural hydrogenation, we demonstrate that structure-sensitive reactions can be used as catalytic probes to investigate the surface structures of heterogeneous catalysts and to understand their structure-property relationships. However again, we emphasize the possibility of the PtSn surface reconstruction under reaction conditions, which may not be observed in many surface characterization techniques such as the CO-DRIFTS used in this work.

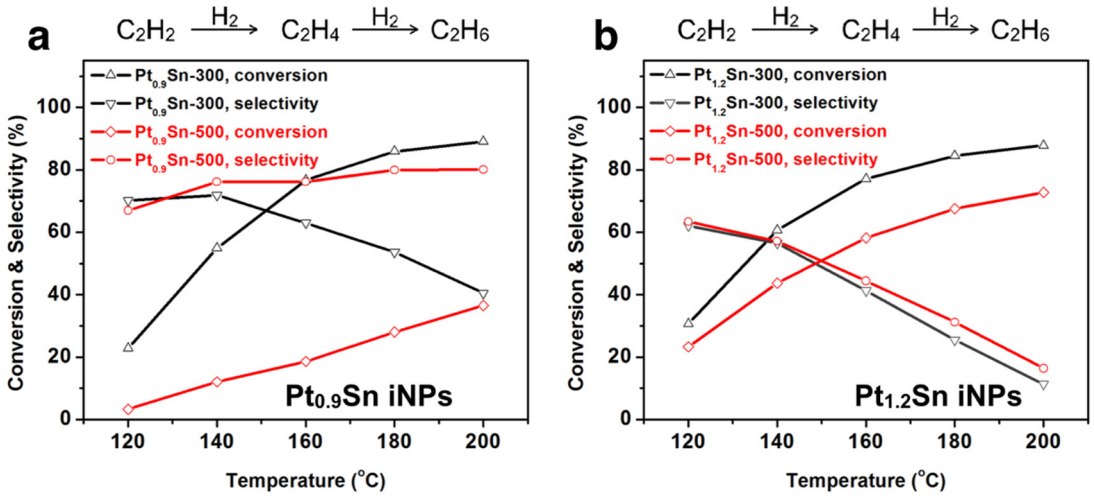

Figure 4. Temperature-dependent conversion and selectivity trends of acetylene semi-hydrogenation over (a) $Pt_{0.9}Sn$ and (b) $Pt_{1.2}Sn$ iNPs reduced at 300 and 500 °C. 2 mg catalyst was used in acetylene semi-hydrogenation with a gas feed of $C_2H_2/C_2H_4/H_2/He$ = 0.15/15/1.5/13.5 mL min^{-1}. Each conversion and selectivity values were calculated by averaging 10 injections.

4. CONCLUSION

In summary, we studied the structure-catalytic property relationship of Pt-Sn iNPs finely tuned as Pt-rich, stoichiometric 1:1, and Sn-rich compositions. The reduction temperature has a strong influence on the structure and catalytic properties of these PtSn iNPs, especially for the Sn-rich $Pt_{0.9}Sn$ iNPs. The furfural hydrogenation and acetylene semi-hydrogenation were used as probes to correlate the surface structure of iNPs to their catalytic properties. Pt-rich $Pt_{1.2}Sn$ iNPs shows higher activity and nevertheless lower selectivity due to the presence of Pt contiguous sites on the surface. Sn-rich $Pt_{0.9}Sn$-300 iNPs have similar Pt contiguous sites on the surface, matching their high activity and low selectivity in probe reactions. At the elevated reduction temperature of 500 °C, $Pt_{0.9}Sn$-500 iNPs shows high selectivity associated with the reduced activity, suggesting an ordered PtSn surface partially covered with Sn atoms. The composition- and reduction temperature-induced surface evolution was also suggested by HAADF-STEM images, EDS line scan, EXAFS, and DRIFTS results.

This study demonstrates the essential roles of composition deviation in intermetallic compounds to significantly affect their surface structures and catalytic properties. We anticipate that the well-ordered intermetallic compounds can be extended to more hydrogenation reactions with appropriate structural design in a predictable manner. We also reveal the importance of a precise composition control of intermetallic nanoparticles on their catalytic properties. Meanwhile, the intermetallic nanoparticles with non-stoichiometric compositions could also lead to another strategy to construct nanostructures satisfying the desired catalysis.

ACKNOWLEDGMENT

This work was partially supported by National Science Foundation (NSF) Grant CHE-1808239. We thank Gordon J. Miller and Matthew Besser for the use of X-ray diffractometer. We thank Igor I. Slowing for the use of Micromeritics AutoChem II 2920. We are grateful to Tianpin Wu, Chengjun Sun, and Lu Ma for their help during the XAFS measurement at station 9-BM-C and 20-BM-B of Advanced Photon Source (APS). The use of APS, an Office of Science User Facility operated for the U.S. Department of Energy (DOE) Office of Science by Argonne National Laboratory, was supported by the U.S. DOE under Contract No. DE-AC02-06CH11357.

REFERENCES

[1] F. Besenbacher, I. Chorkendorff, B.S. Clausen, B. Hammer, A.M. Molenbroek, J.K. Norskov, I. Stensgaard, Science 279 (1998) 1913-1915.

[2] J. Shan, S. Zhang, T. Choksi, L. Nguyen, C. Bonifacio, Y. Li, W. Zhu, Y. Tang, J.C. Yang, J. Greeley, A.I. Frenkel, F. Tao, ACS. Catal. 7 (2017) 191-204.

[3] J.J.F. Scholten, A.P. Pijpers, A.M.L. Hustings, Catal. Rev. 27 (1985) 151-206.

[4] J.K.A. Clarke, Chem. Rev. 75 (1975) 291-305.

[5] W.T. Yu, M.D. Porosoff, J.G.G. Chen, Chem. Rev. 112 (2012) 5780-5817.

[6] R. Ferrando, J. Jellinek, R.L. Johnston, Chem. Rev. 108 (2008) 845-910.

[7] S.J. Guo, S. Zhang, S.H. Sun, Angew. Chem. Int. Ed. 52 (2013) 8526-8544.

[8] J.A. Rodriguez, Surf. Sci. Rep. 24 (1996) 225-287.

[9] F. Tao, M.E. Grass, Y. Zhang, D.R. Butcher, J.R. Renza, Z. Liu, J.Y. Chung, B.S. Mun, M. Salmeron, G.A. Somorjai, Science 322 (2008) 932-934.
[10] H. Zhang, M.S. Jin, J.G. Wang, W.Y. Li, P.H.C. Camargo, M.J. Kim, D.R. Yang, Z.X. Xie, Y.A. Xia, J. Am. Chem. Soc. 133 (2011) 6078-6089.
[11] M.A. Mahmoud, F. Saira, M.A. El-Sayed, Nano Lett. 10 (2010) 3764-3769.
[12] Y. Yang, J.Y. Liu, Z.W. Fu, D. Qin, J. Am. Chem. Soc. 136 (2014) 8153-8156.
[13] E. Herrero, L.J. Buller, H.D. Abruna, Chem. Rev. 101 (2001) 1897-1930.
[14] G. Kokkinidis, J Electroanal Chem. 201 (1986) 217-236.
[15] J. Greeley, T.F. Jaramillo, J. Bonde, I.B. Chorkendorff, J.K. Norskov, Nat. Mater. 5 (2006) 909-913.
[16] F. Maury, A. Lucasson, P. Lucasson, P. Moser, Y. Loreaux, J. Phys. F. Met. Phys. 15 (1985) 1465-1484.
[17] J. Greeley, M. Mavrikakis, Nat. Mater. 3 (2004) 810-815.
[18] A. Van der Ven, G. Ceder, Phys. Rev. Lett. 94 (2005) 045901.
[19] L.A. Girifalco, J. Phys. Chem. Solids 25 (1964) 323-333.
[20] K.H.J. Buschow, Rep. Prog. Phys. 40 (1977) 1179-1256.
[21] M. Armbruster, R. Schlogl, Y. Grin, Sci. Technol. Adv. Mater. 15 (2014) 034803.
[22] J.R. Gallagher, D.J. Childers, H.Y. Zhao, R.E. Winans, R.J. Meyer, J.T. Miller, Phys. Chem. Chem. Phys. 17 (2015) 28144-28153.
[23] S. Furukawa, T. Komatsu, ACS Catal. 7 (2017) 735-765.
[24] R.V. Maligal-Ganesh, C. Xiao, T.W. Goh, L.-L. Wang, J. Gustafson, Y. Pei, Z. Qi, D.D. Johnson, S. Zhang, F. Tao, W. Huang, ACS Catal. 6 (2016) 1754-1763.
[25] H. Zhou, X. Yang, L. Li, X. Liu, Y. Huang, X. Pan, A. Wang, J. Li, T. Zhang, ACS Catal. 6 (2016) 1054-1061.
[26] H.R. Zhou, X.F. Yang, L. Li, X.Y. Liu, Y.Q. Huang, X.L. Pan, A.Q. Wang, J. Li, T. Zhang, ACS Catal. 6 (2016) 1054-1061.
[27] J. Prinz, R. Gaspari, C.A. Pignedoli, J. Vogt, P. Gille, M. Armbrüster, H. Brune, O. Gröning, D. Passerone, R. Widmer, Angew. Chem. Int. Ed. 51 (2012) 9339-9343.
[28] D.Y. DeSario, F.J. DiSalvo, Chem. Mater. 26 (2014) 2750-2757.
[29] J.C. Bauer, X. Chen, Q. Liu, T.-H. Phan, R.E. Schaak, J. Mater. Chem. 18 (2008) 275-282.
[30] Z.Y. Qi, C.X. Xiao, C. Liu, T.W. Goh, L. Zhou, R. Maligal-Ganesh, Y.C. Pei, X.L. Li, L.A.

Curtiss, W.Y. Huang, J. Am. Chem. Soc. 139 (2017) 4762-4768.
[31] s. Cai, H. Duan, H. Rong, D. Wang, L. Li, W. He, Y. Li, ACS Catal. 3 (2013) 608-612.
[32] C. Chen, Y. Kang, Z. Huo, Z. Zhu, W. Huang, H.L. Xin, J.D. Snyder, D. Li, J.A. Herron, M. Mavrikakis, M. Chi, K.L. More, Y. Li, N.M. Markovic, G.A. Somorjai, P. Yang, V.R. Stamenkovic, Science 343 (2014) 1339-1343.
[33] Z. Liu, G.S. Jackson, B.W. Eichhorn, Angew. Chem. Int. Ed. 49 (2010) 3173-3176.
[34] Q.C. Feng, S. Zhao, Y. Wang, J.C. Dong, W.X. Chen, D.S. He, D.S. Wang, J. Yang, Y.M. Zhu, H.L. Zhu, L. Gu, Z. Li, Y.X. Liu, R. Yu, J. Li, Y.D. Li, J. Am. Chem. Soc. 139 (2017) 7294-7301.
[35] J. Prinz, R. Gaspari, C.A. Pignedoli, J. Vogt, P. Gille, M. Armbruster, H. Brune, O. Groning, D. Passerone, R. Widmer, Angew. Chem. Int. Ed. 51 (2012) 9339-9343.
[36] S. Iihama, S. Furukawa, T. Komatsu, ACS Catal. 6 (2016) 742-746.
[37] Y.C. Pei, Z.Y. Qi, T.W. Goh, L.L. Wang, R.V. Maligal-Ganesh, H.L. MacMurdo, S.R. Zhang, C.X. Xiao, X.L. Li, F. Tao, D.D. Johnson, W.Y. Huang, J. Catal. 356 (2017) 307-314.
[38] H. Okamoto, J Phase Equilib 24 (2003) 198-198.
[39] Y. Pei, R.V. Maligal-Ganesh, C. Xiao, T.W. Goh, K. Brashler, J.A. Gustafson, W. Huang, Nanoscale 7 (2015) 16721-16728.
[40] E.W. Zhao, R. Maligal-Ganesh, C. Xiao, T.W. Goh, Z. Qi, Y. Pei, H.E. Hagelin-Weaver, W. Huang, C.R. Bowers, Angew. Chem. Int. Ed. 56 (2017) 3925-3929.
[41] A. Borodzinski, M. Bonarowska, Langmuir 13 (1997) 5613-5620.
[42] H. Verbeek, W.M.H. Sachtler, J. Catal. 42 (1976) 257-267.
[43] Y. Uemura, Y. Inada, K.K. Bando, T. Sasaki, N. Kamiuchi, K. Eguchi, A. Yagishita, M. Nomura, M. Tada, Y. Iwasawa, Phys. Chem. Chem. Phys. 13 (2011) 15833-15844.
[44] N. Murata, T. Suzuki, M. Kobayashi, F. Togoh, K. Asakura, Phys. Chem. Chem. Phys. 15 (2013) 17938-17946.
[45] Pt-Sn (PtSn) Crystal Structure: Datasheet from "PAULING FILE Multinaries Edition – 2012" in SpringerMaterials (http://materials.springer.com/isp/crystallographic/docs/sd_1822402), in, Springer-Verlag Berlin Heidelberg & Material Phases Data System (MPDS), Switzerland & National Institute for Materials Science (NIMS), Japan.
[46] K. Sasaki, H. Naohara, Y. Cai, Y.M. Choi, P. Liu, M.B. Vukmirovic, J.X. Wang, R.R. Adzic,

Angew. Chem. Int. Ed. 49 (2010) 8602-8607.
[47] S. Xie, S.I. Choi, N. Lu, L.T. Roling, J.A. Herron, L. Zhang, J. Park, J. Wang, M.J. Kim, Z. Xie, M. Mavrikakis, Y. Xia, Nano Lett. 14 (2014) 3570-3576.
[48] J. Fearon, G.W. Watson, J. Mater. Chem. 16 (2006) 1989-1996.
[49] Y.X. Yao, Q. Fu, Z. Zhang, H. Zhang, T. Ma, D. Tan, X.H. Bao, Appl. Surf. Sci. 254 (2008) 3808-3812.
[50] J. Yang, F.J. Zhang, H.Y. Lu, X. Hong, H.L. Jiang, Y. Wu, Y.D. Li, Angew. Chem. Int. Ed. 54 (2015) 10889-10893.
[51] J. Osswald, K. Kovnir, M. Armbruster, R. Giedigleit, R.E. Jentoft, U. Wild, Y. Grin, R. Schlogl, J. Catal. 258 (2008) 219-227.
[52] H. Wei, X. Liu, A. Wang, L. Zhang, B. Qiao, X. Yang, Y. Huang, S. Miao, J. Liu, T. Zhang, Nat. Commun. 5 (2014) 5634.